Ocean Dynamics (2010) 60:317–330
DOI 10.1007/s10236-009-0245-y

Estimation of the internal pressure gradient in σ-coordinate ocean models: comparison of second-, fourth-, and sixth-order schemes

Jarle Berntsen · Lie-Yauw Oey

Received: 10 July 2009 / Accepted: 6 November 2009 / Published online: 20 November 2009

Abstract Sigma-coordinate ocean models are attractive because of their abilities to resolve bottom and surface boundary layers. However, these models can have large internal pressure gradient (IPG) errors. In this paper, two classes of methods for the estimation of the IPGs are assessed. The first is based on the integral approach used in the Princeton Ocean Model (POM). The second is suggested by Shchepetkin and McWilliams (2003) based on Green's theorem; thus, area integrals of the pressure forces are transformed into line integrals. Numerical tests on the seamount problem, as well as on a northwestern Atlantic grid using both classes of methods, are presented. For each class, second-, fourth-, and sixth-order approximations are tested. Results produced with a fourth-order compact method and with cubic spline methods are also given. The results show that the methods based on the POM approach in general give smaller errors than the corresponding methods given in Shchepetkin and McWilliams (2003). The POM approach also is more robust when noise is added to the topography. In particular, the IPG errors may be substantially reduced by using the computationally simple fourth-order method from McCalpin (1994).

Responsible Editor: Tal Ezer

J. Berntsen (✉)
Department of Mathematics, University of Bergen,
Johannes Brunsgate 12, 5008 Bergen, Norway
e-mail: jarle.berntsen@math.uib.no

L.-Y. Oey
Program in Atmospheric and Oceanic Sciences,
Princeton University, Princeton, NJ, USA

Keywords Ocean modeling · Sigma-coordinates · Internal pressure

1 Introduction

Sigma coordinate ocean models, or models based on more generalized terrain-following coordinate systems, are widely used in oceanographic studies, see for instance Kantha and Clayson (2000). In σ-coordinate ocean models, the x-component of the internal density gradient may, after neglecting the free surface elevation, be written

$$\left.\frac{\partial \rho}{\partial x}\right|_z = \frac{\partial \rho}{\partial x} - \frac{\sigma}{H}\frac{\partial H}{\partial x}\frac{\partial \rho}{\partial \sigma}, \tag{1}$$

where x is the horizontal coordinate, z the vertical coordinate, ρ the density, H the depth, and $\sigma \equiv z/H$. Near steep topography, the two terms on the right-hand side of Eq. 1 may be large and comparable in magnitude. The difference of two large terms may cause large errors in the estimates of the internal pressure gradient.

Over the years, there has been some controversy over the concept "hydrostatic consistency," see Haney (1991). A scheme is said to be hydrostatically consistent if

$$\left|\frac{\sigma}{\delta\sigma}\frac{\delta_x H}{H}\right| < 1\ . \tag{2}$$

In Eq. 2, $\delta\sigma$ is the discrete sigma layer thickness and δ_x is the discrete difference operator in the x-direction. For non-zero σ, a σ-model becomes

hydrostatically inconsistent when $\delta\sigma$ tends to zero. Mellor et al. (1994) derived the following discretization error for the second-order internal pressure method used in the Princeton Ocean Model (POM) (Blumberg and Mellor 1987; Mellor 2003):

$$\mathrm{E}\left(\frac{\delta_x b}{\delta x}\right) = \frac{H}{4}\frac{\delta_x H}{\delta x}\left(\frac{\partial^2 b}{\partial z^2}\right)\left\{(\delta\sigma)^2 - \sigma^2\left(\frac{\delta_x H}{H}\right)^2\right\}, \tag{3}$$

where $b = \rho g/\rho_0$, g is the gravity constant, and ρ_0 is a constant reference density; Eq. 3 shows that the error decreases as $\delta\sigma$ and $\delta_x H$ both tend to zero, contrary to that implied by Eq. 2. It also shows that, for a given σ and $\delta_x H/H$, the error does not become large as $\delta\sigma$ tends to zero. Therefore, hydrostatic consistency is not a useful concept. The error term Eq. 3 suggests that the truncation errors may be reduced if higher-order schemes are used. Furthermore, the error behaviors may strongly depend on the particular discretization scheme used.

Mellor et al. (1994) showed that, in diagnostic experiments, the pressure errors are maintained in time as an input of potential energy, and the mean kinetic energy does not tend to zero even if the system is not externally forced. However, in two-dimensional (x, z) prognostic experiments, the density field is advectively adjusted, the numerical potential energy tends to zero, and the mean kinetic energy accordingly dies out.

Beckmann and Haidvogel (1993) studied flow over a three-dimensional seamount. For their internal pressure gradient (IPG) scheme, the vorticity resulting from the IPGs grew indefinitely in time. For the same seamount problem, Mellor et al. (1998) reported that the errors asymptote to constants in time. Mellor et al. (1998) categorized the errors reported in Mellor et al. (1994) as sigma errors of the first kind (SEFK). These errors are associated with two-dimensional (x, z) flow. They categorized the vorticity errors reported by Beckmann and Haidvogel as sigma errors of the second kind (SESK). For the SEFK, the internal pressure errors create first errors in the velocities, which die out as a compensating error in the density field develops. For the SESK case, the velocities driven by the perturbed density field asymptote to constant values in time.

The IPG errors may be reduced by increasing the values of the eddy viscosities, see for instance Mellor et al. (1998), Berntsen (2002), and Shchepetkin and McWilliams (2003) (SM03). The errors may also be reduced by subtracting the background stratification, $\rho_{\mathrm{ref}}(z)$, or some fraction of it, see Gary (1973) and Mellor et al. (1998). The erroneous flow may be reduced to any level in idealized studies where the density is a function of z only by subtracting $\rho_{\mathrm{ref}}(z)$. For the case of $\rho = \rho(z)$, for instance, one may choose $\rho_{\mathrm{ref}}(z) = \rho(z)$ and there will be no erroneous IPGs. Therefore, to get an idea of the magnitude of the artificial flow in experiments with more realistic IPGs, one may avoid subtraction of $\rho_{\mathrm{ref}}(z)$ as in Barnier et al. (1998), Berntsen (2002), and SM03. The subtraction of a background density profile may create erroneous pressure gradients also for a homogeneous ocean. In Robertson et al. (2001), this problem is discussed and methods for eliminating the errors associated with the subtraction of a background density profile are given. In the studies to be described in the present paper, $\rho_{\mathrm{ref}}(z)$ is not subtracted. A third technique to reduce the IPG errors is to smooth the topography or to reduce $\frac{\delta_x H}{\delta x}$, see Mellor et al. (1994), Barnier et al. (1998), and Sikirić et al. (2009). When smoothing the topography, results for a model domain different from the physical domain will be produced. This will create an additional source of errors, and the errors due to topography smoothing should ideally be quantified if this approach is chosen. In Di Lorenzo et al. (2006), for instance, it is demonstrated that topography smoothing may affect the conversion of energy from the barotropic tides to the internal tides.

Stelling and Van Kester (1994) suggested that the IPG errors may be reduced by interpolating the density back to z-levels to calculate the pressure gradient force. The Stelling and Van Kester (1994) method is the only method that guarantees that the estimated IPGs are zero when the real pressure gradients are zero. However, Slørdal (1997) stated that the pressure gradient force may be underestimated using this approach and suggested linear interpolation in the vertical. For further discussions on z-level methods, see Kliem and Pietrzak (1999), Ciappa (2006), and Fortunato and Baptista (1996).

New algorithms that attempt to reduce the size of the internal pressure errors are presented in several papers. McCalpin (1994) and Chu and Fan (1997, 2003) proposed using higher-order approximations. Weighted Jacobian methods have also been suggested, see Song (1998) and Song and Wright (1998). In the POM, and most other σ-coordinate models, the internal pressure forces are computed by estimating vertical integrals of Eq. 1. SM03 proposed using Green's theorem. In their approach, area integrals of the pressure forces acting on the cells surrounding the velocity points are transformed into corresponding line integrals. The line integrals are computed using exact integrations of polynomial fits of the integrands. SM03 show that the methods based on the use of cubic splines perform very favorably.

The growth of the IPG errors may depend also on components of the ocean models other than the estimates of the pressure forces (Berntsen and Furnes 2005). In the present paper, we investigate if the general conclusions from SM03 may be extended to other terrain-following models. In particular, we wish to clarify if the good performance reported in SM03 was due to the use of Green's theorem approach or to the use of higher-order methods. Furthermore, the role of the vertical approximation methods vs the horizontal methods will be clarified.

Ezer et al. (2002) also tested different IPG methods for the seamount case, including some of the SM03 methods. However, the results are inconclusive in part because different models (POM and ROMS) were used for different methods. In the present study, all tests are performed using the same ocean model (POM). We also expand the range of methods and integration time, and also examine effects to IPG errors for the seamount with noise added to the topography. Additionally, the IPG errors for a model with realistic topography (northwest Atlantic) are evaluated.

2 The two approaches

In this section, the two approaches for estimation of the IPG forces in σ-coordinate ocean models are described. In the POM, vertical integrals are used to estimate the IPGs, and this will be denoted as the POM approach.

2.1 POM approach

After including the effects of the free surface elevation η, the x-component of the IPG term may be written

$$-\frac{1}{\rho_0}\left.\frac{\partial p}{\partial x}\right|_z = -\frac{gD}{\rho_0}\int_\sigma^0 \left(\frac{\partial \rho}{\partial x} - \frac{\sigma}{D}\frac{\partial D}{\partial x}\frac{\partial \rho}{\partial \sigma}\right) d\sigma, \tag{4}$$

where $D = H + \eta$ and H is the undisturbed water depth and $\sigma \equiv \frac{z-\eta}{D}$. Utilizing integration by parts on the second term under the integral above according to

$$\int_\sigma^0 \sigma \frac{\partial \rho}{\partial \sigma} d\sigma = -\sigma\rho - \int_\sigma^0 \rho d\sigma\,, \tag{5}$$

the IPG term may be rewritten as

$$-\frac{1}{\rho_0}\left.\frac{\partial p}{\partial x}\right|_z = -\frac{gD}{\rho_0}\left[\int_\sigma^0 \left(\frac{\partial \rho}{\partial x} + \frac{1}{D}\frac{\partial D}{\partial x}\rho\right) d\sigma + \frac{\sigma\rho}{D}\frac{\partial D}{\partial x}\right]. \tag{6}$$

The strategy in C-grid models like the POM is to approximate the pressure forces (Eq. 4) in the velocity points of the model, using second-order differences on the derivatives and the trapezoidal rule on the vertical integrals. It is mathematically equivalent to basing the discretization on Eq. 4 or Eq. 6. The integrand in Eq. 6 is somewhat less complicated, the $\frac{\partial \rho}{\partial \sigma}$ term in Eq. 4 is replaced by ρ. This simplifies the computations slightly, especially when introducing higher-order methods on the integrations. The studies to be presented are based on discretizations of Eq. 6.

2.2 Green's theorem approach

In SM03, the area integrals of the pressure forces acting on the cells surrounding the velocity points are transformed into corresponding line integrals around the surrounding cells according to

$$\int_A \int \left.\frac{\partial \rho}{\partial x}\right|_z dx dz = \oint \rho \mathbf{dz} \tag{7}$$

using Green's theorem. Statement 7 is the same as (2.14) in SM03. Using this approach, they approximate the contour integrals in the right-hand side of Eq. 7 using analytic integrations. This leads them to their Cubic-A and Cubic-H methods, which apply algebraic and harmonic averaging of the derivatives at the end points of the intervals, respectively. For details, see Section 5 in SM03.

2.3 The comparison

In order to examine possible benefits from Green's theorem approach, a sequence of studies where the approximations in both approaches are taken to the same order of accuracy is performed. To second order, both methods become identical, and therefore, higher order is necessary to clarify the differences.

The fourth-order methods used for the POM approach are the McCalpin method and a method based on compact differencing, see Orzag and Israeli (1974). The compact differencing fourth-order method is implicit and requires the solution of tridiagonal systems of equations. However, there is numerical evidence (Orzag and Israeli 1974) that the errors may be substantially reduced by using this technique. For the SM03 class of methods, the method based on four-point cubic polynomial fit (their statements (5.5) and (5.6)) is used in addition to the Cubic-H and Cubic-A methods.

Table 1 List of acronyms

Acronym	Method	Computation time (in s)
pom2nd	POM standard 2nd order	52.3
pom4thMcC	POM 4th order McCalpin	55.4
pom4thCmp	POM 4th order compact differencing	68.1
pom6th	POM 6th order Chu and Fan	62.1
sm4thpoly	SM03 4th order polynomial interpolation	56.0
sm4thCubicH	SM03 4th order Cubic H	56.7
sm4thCubicA	SM03 4th order Cubic A	56.2
sm6th	SM03 6th order polynomial interpolation	74.4

The computation times are for 2 days of integration over a $65 \times 49 \times 51$ grid for the seamount problem with an internal time step of 180 s using a serial code on an Intel OPTIPLEX 760 PC

To sixth order, the method described in Chu and Fan (1997) is used for the POM approach. The methods from SM03 are also extended to sixth order to facilitate a comparison, see Appendix for details.

The focus in the present paper is on the sensitivity of the errors to the horizontal approximations. The sensitivity of the errors to the choice of vertical integration method is less, but these errors will also be presented. In Table 1, a list of acronyms for the various methods is given to simplify the referencing in the following text.

3 The seamount case

The seamount problem was defined by Beckmann and Haidvogel (1993) and later used in many papers, see for instance Mellor et al. (1998), Shchepetkin and McWilliams (2003), and Berntsen and Furnes (2005).

The bottom topography in the present studies is defined as

$$H(x, y) = H_0(1.0 - 0.90e^{-(x^2+y^2)/L^2}) , \tag{8}$$

where $H_0 = 4{,}500$ m and $L = 40$ km. The seamount is placed in the center of a channel that is 390 km long in the x-direction and 294 km wide in the y-direction. The channel is closed at $x = 0$ km and $x = 390$ km, and at $y = 0$ km and $y = 294$ km.

The horizontal grid size is constant and equal to 6 km. The Coriolis parameter is constant and equal to 10^{-4} s^{-1}. The horizontal viscosity, A_M, is set equal to 100 m^2 s^{-1} and the horizontal viscous terms are written as in Mellor et al. (1998). The horizontal and vertical diffusivities are zero in the present experiments.

An initial exponential stratification is assumed

$$\rho(z) = \rho_b - \Delta\rho e^{z/500\ \mathrm{m}} , \tag{9}$$

where z is the upward distance from the surface in meters, $\rho_b = 28$ kg m^{-3}, and $\Delta\rho = 3.263$ kg m^{-3}. The Burger number

$$S = \frac{\sqrt{gH_0\Delta\rho/\rho_0}}{fL} \tag{10}$$

becomes 3.0 for the present set of parameters. The perturbation density ρ' (in kg m^{-3}) is initially defined as

$$\rho'(z) = 1.5\, e^{z/500\ \mathrm{m}} . \tag{11}$$

Following Mellor et al. (1998), see also Beckmann and Haidvogel (1993), the perturbation density is solved using the linearized equations to isolate the IPG errors. By using linearized equations, we can, for example, set the horizontal diffusivities to zero and avoid diapycnal mixing that may complicate the interpretations of the IPG errors. The perturbation density ρ' is also used to estimate the IPGs.

The velocities and the water elevation are initially zero, and there is no physical forcing in this case. The true solution is no flow.

In the numerical experiments, the following diagnostic measures, see Mellor et al. (1994, 1998), and SM03, are monitored:

kinetic energy,

$$E_{\mathrm{kin}} = \frac{1}{2V}\sum_{i,j,k}\left[\Delta V_{i+\frac{1}{2},j,k}u^2_{i+\frac{1}{2},j,k} + \Delta V_{i,j+\frac{1}{2},k}v^2_{i,j+\frac{1}{2},k}\right] , \tag{12}$$

and maximum velocity,

$$V_{\max} = \max\left[u_{i+\frac{1}{2},j,k}, v_{i,j+\frac{1}{2},k}\right] . \tag{13}$$

In the equations above,

$$V = \sum_{i,j,k}\Delta V_{i,j,k} , \tag{14}$$

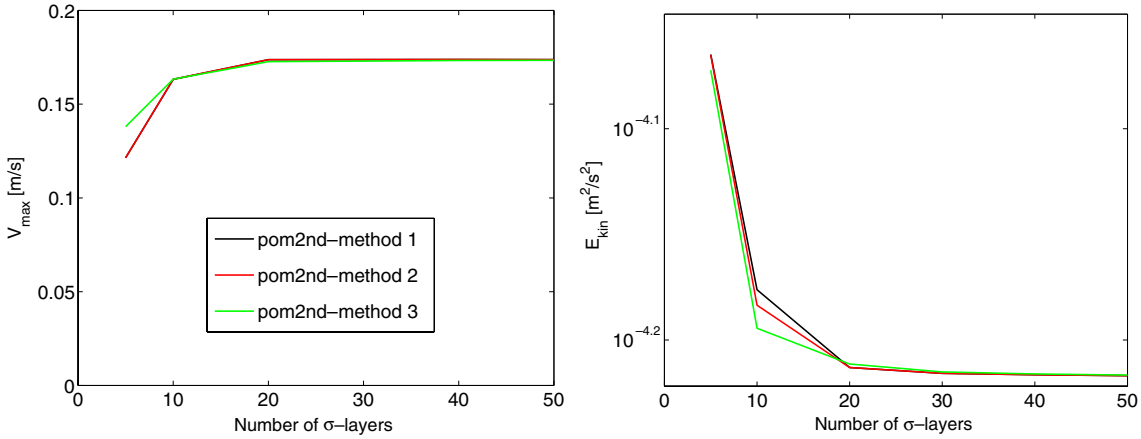

Fig. 1 The maximum velocities $V_{\max}$ after 10 days are given in **a**, and the kinetic energies E_{kin} are given in **b** as functions of the number of equidistant σ-layers for the three vertical integration methods. The pom2nd method is used for the horizontal approximations

is the total volume of the domain, and $\Delta V_{i,j,k}$, $\Delta V_{i+\frac{1}{2},j,k}$, and $\Delta V_{i,j+\frac{1}{2},k}$ are control volumes of ρ, u, and v point grid boxes, respectively.

3.1 Sensitivity of the errors to the vertical discretization method

To investigate the sensitivity of the errors to the estimation of the vertical integrals, the kinetic energies and maximum velocities after 10 days are given in Fig. 1 for the following vertical integration methods

1. The trapezoidal rule as in the POM.
2. The trapezoidal rule over all interior intervals and the assumption of a linear density profile is used to integrate over the top half cell, see Remark 4 in Section 5.1 in SM03.
3. The vertical integrals are estimated to fourth-order accuracy, except for the bottom and top integrals, which are estimated to second order.

The number of equidistant σ-layers is varied from 5 to 50.

Figure 1 shows that the results are insensitive to the choice of vertical integration method, and the results for methods 1 and 2 are hardly distinguishable. The results produced with 20, 30, 40, and 50 equidistant σ-layers are almost identical when using the pom2nd method for the horizontal approximations. This is consistent with the discussion of the error term Eq. 3 given

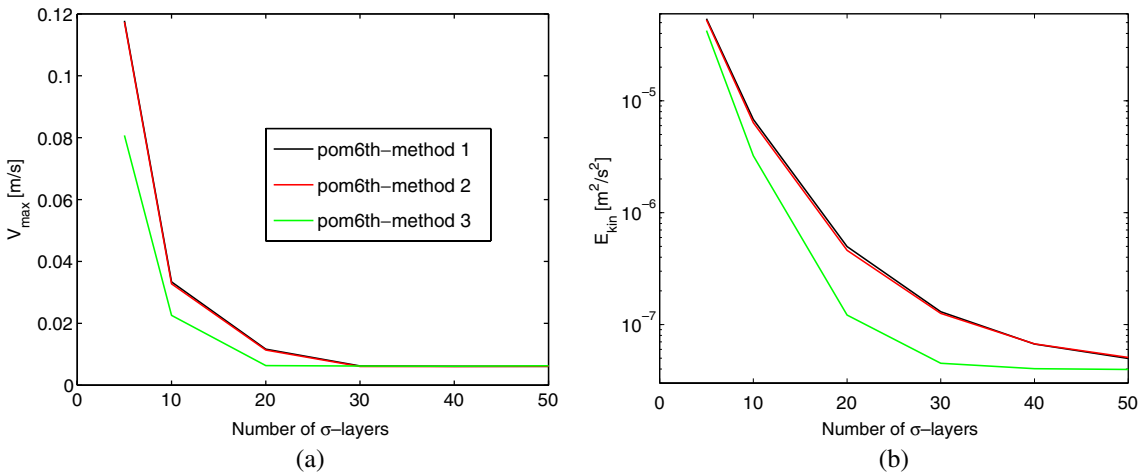

Fig. 2 Same as Fig. 1, but the pom6th method is used for the horizontal approximations

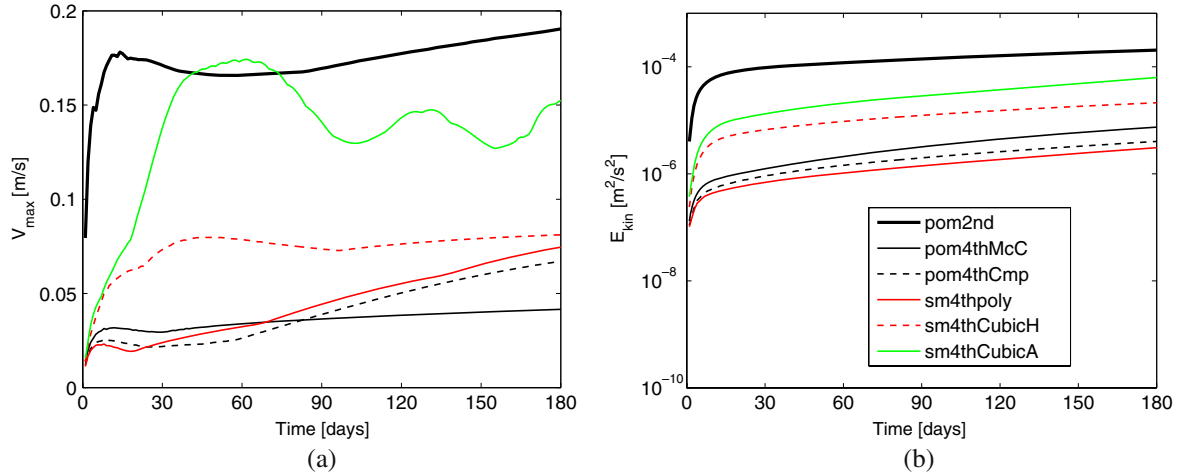

Fig. 3 Time series of $V_{\max}$ and E_{kin} for the pom2nd method and the five fourth-order methods (**a**, **b**)

in Section 1. In other words, the "hydrostatic consistency" condition Eq. 2 does not seem to be relevant.

When applying higher-order approximations horizontally, one may expect that the vertical integration errors may become more important, and that more vertical layers are needed to benefit from the improved horizontal approximations. To demonstrate this, the exercise of Fig. 1 is repeated with the pom6th method, see Fig. 2. The effects of using a second-order method over the upper half cell, method 2, are, again, very small. Figure 2 shows that, with increased horizontal accuracy using the sixth-order scheme, there is a clear reduction in IPG errors when the fourth-order vertical scheme is used, especially at relatively coarse $\delta\sigma$. With an increased number of σ-layers, the improvement is less.

3.2 Sensitivity of the errors to the horizontal discretization method

We next focus on the horizontal approximations and compare the fourth-order POM-type methods and fourth-order SM03 methods. Time series of maximum velocities and kinetic energies are given in Fig. 3. These experiments are performed with 40 equidistant layers. With this vertical grid spacing, the horizontal discretization errors dominate and the standard

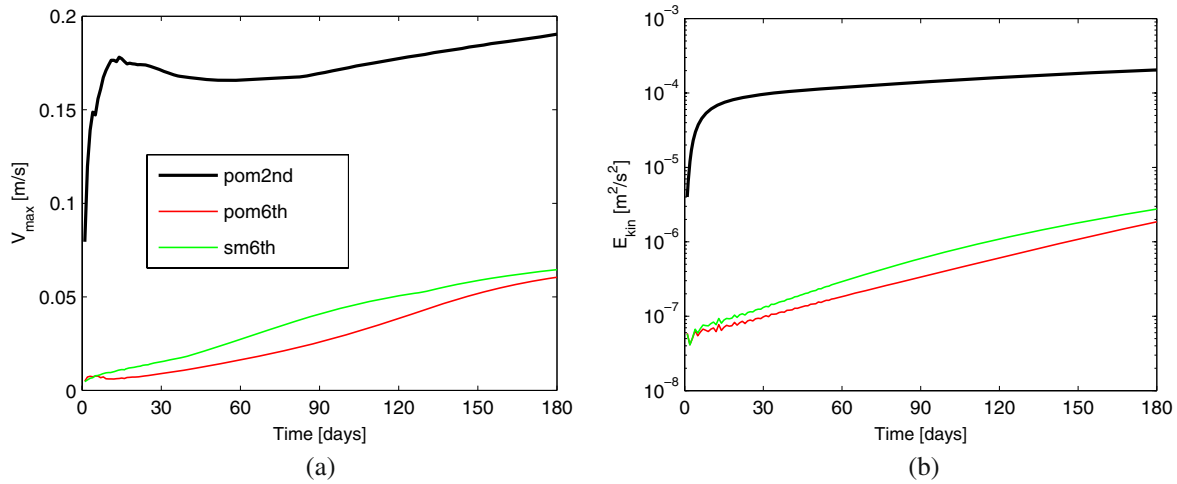

Fig. 4 Time series of $V_{\max}$ and E_{kin} for the pom2nd method and the two sixth-order methods (**a**, **b**)

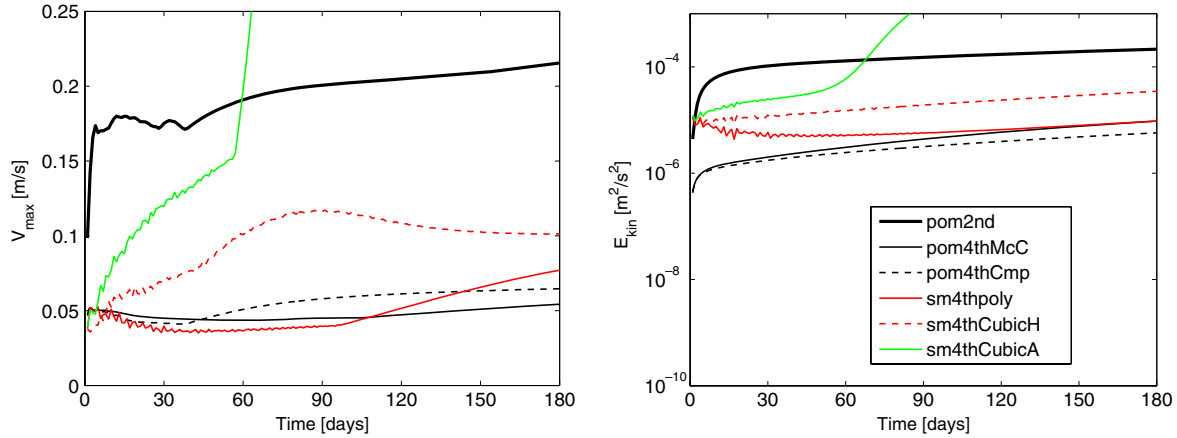

Fig. 5 Same as Fig. 3, but for the experiments with uniformly distributed noise added to the bottom topography (**a**, **b**)

trapezoidal rule is applied vertically. The errors are generally reduced when applying the fourth-order horizontal approximations. The sm4thCubicA method clearly produces larger errors than the other fourth-order methods, and the sm4thpoly method, the pom4thMcC method, and the pom4thCmp method all perform well in this test case. In SM03, it is argued that the fourth-order polynomial fit method did create spurious oscillations in the polynomial fits to the density profiles and that oscillations are avoided when using the Cubic-H method. In view of these arguments, it is surprising that the errors produced with the sm4thpoly method are smaller than the corresponding errors produced with the sm4thCubicH method.

The results for the sixth-order methods for both the POM and SM03 are similar, see Fig. 4, with slightly smaller errors for the POM method. On a short time scale, the errors for the sixth-order methods are smaller than the errors for the fourth-order methods (cf. Fig. 3), but the former errors increase with time. Therefore, it may not be beneficial to use the sixth-order schemes for long time integrations. To investigate the sensitivity of the results to a noisy topography, the above calculations are repeated by perturbing the smooth seamount topography (Eq. 8) according to

$$H(x, y) = H_0(1.0 - 0.90e^{-(x^2+y^2)/L^2}) - 50\,\mathrm{m} \times r\,, \quad (15)$$

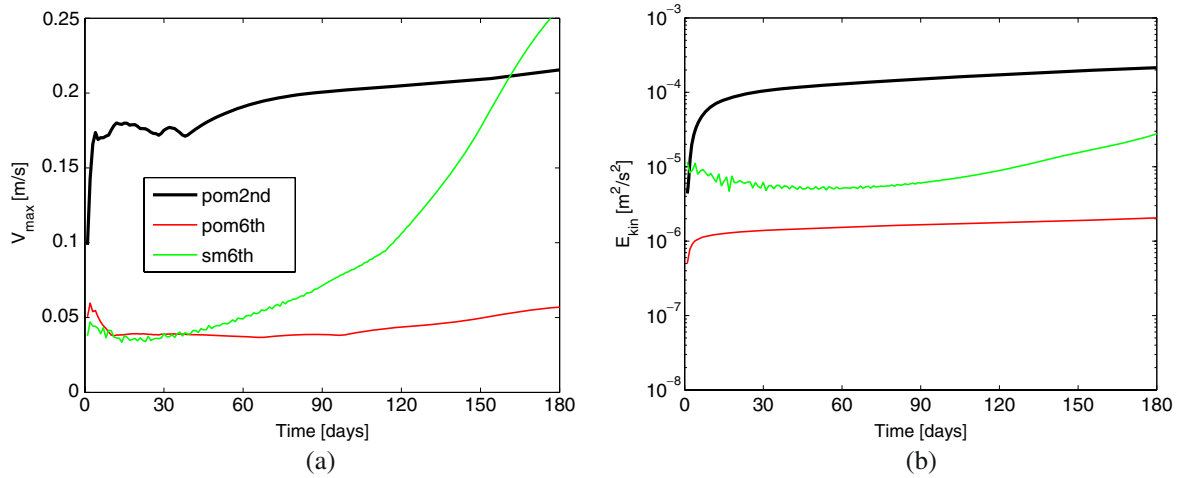

Fig. 6 Same as Fig. 4, but for the experiments with uniformly distributed noise added to the bottom topography (**a**, **b**)

where r is a random number uniformly distributed between 0 and 1. For each experiment, the same sequence of random numbers is used. The maximum velocities and kinetic energies for these experiments are given in Figs. 5 and 6. The POM methods are, in general, more robust to the added noise than the SM03 methods. By comparing the results for the sixth-order methods (Figs. 4 and 6), we notice that the errors grow faster in the later set of experiments for the sm6th method. This finding is in agreement with the general experience in numerical modeling that higher-order methods are most favorable on smooth, analytical problems. On the other hand, the pom6th method is surprisingly well-behaved (Fig. 6). The effects of the added noise on the results for the fourth-order methods fall between the corresponding effects on the second- and sixth-order methods. The growth of the errors produced with the sm4thCubicA method becomes, however, very large in the noisy topography case (Fig. 5).

4 The Northwest Atlantic case

To assess the IPG errors in a typical oceanic application with realistic bathymetry, we apply the above analysis to a model of the northwestern Atlantic Ocean: 5–50°N and 55–98°W on an orthogonal curvilinear grid. The topography is from the US Navy's DBDB2 v2.2 dataset linearly interpolated onto the grid. The grid is similar to that used in Oey et al. (2003); however, to accentuate the IPG errors, the horizontal grid sizes are doubled (i.e., coarser), so that they are approximately 20 km in the Atlantic Ocean and in the Gulf of Mexico, and about 40 km in the Caribbean Sea. The same 25, non-uniform sigma levels are used in the vertical, finer near the bottom and surface. Results from POM and SM03 methods will be presented, except the sm4thCubicA, which gave excessively large errors, and which became unstable.

The same initial stratification (Eq. 9) as that used for the seamount case is used. The perturbation density is made ten times smaller, i.e., $\rho' = 0.15e^{z/500\ \mathrm{m}}$, which is more typical of the oceanic conditions. In a linear solution, the pressure gradient error is proportional to ρ', so the results below may be scaled appropriately for different values of ρ'. Because of the coarser grid, the horizontal viscosity is also made five times larger, i.e., $A_M = 500\ \mathrm{m^2\ s^{-1}}$. Other model set-ups are otherwise identical to the seamount case: The linearized equations from Mellor et al. (1998) are integrated in time with no physical forcing, and the initial state is a fluid at rest. In each of the following tests, the model was integrated for 180 days (note: the reference density is not removed when computing the IPG). The domain is closed on all four sides so that, as in the seamount problem, the exact solution in the absence of forcing is a quiescent fluid.

The maximum velocities and kinetic energies for the Northwest Atlantic experiments are compared in Fig. 7. The SM03 methods, the sm4thCubicH method in particular, initially give smaller errors. However, these errors grow with time, and by day 120, all the fourth-order methods show comparable $V_{\max}$, which are smaller than the $V_{\max}$ for the pom2nd method by approximately a factor of two. The $V_{\max}$ for the fourth-order POM methods reaches a minimum of less

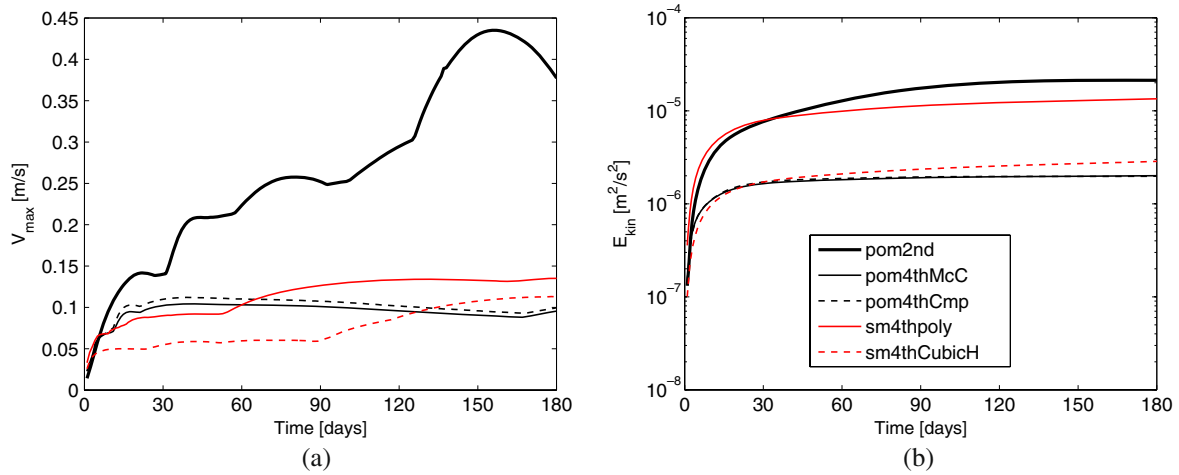

Fig. 7 Time series of $V_{\max}$ and E_{kin} for the Northwest Atlantic experiment for the pom2nd method and four fourth-order methods (**a**, **b**)

than 0.1 m s^{-1} near day 170 before increasing through day 180. The V_{max} for the fourth-order SM03 methods increases with time, as does also V_{max} for the second-order POM. In pom2nd, however, the V_{max} decreases with further time integration.

The domain-averaged kinetic energy, E_{kin}, is comparable for the fourth-order POM methods (McCalpin and compact differencing give virtually identical errors) and the sm4thCubicH method, see Fig. 7b, with the fourth-order POM giving slightly smaller E_{kin} than the sm4thCubicH. Consistent with the results for the V_{max} errors in Fig. 7a, the fourth-order POM methods show errors that asymptote to a constant value. The SM03 fourth-order Cubic-H method shows an increasing-error behavior. We will show below (Fig. 9) that the SM03 methods in general also give larger errors over wider regions than the POM-type methods. This explains why the E_{kin} errors in both methods are comparable at all times, with the sm4thCubicH error being slightly larger after day 180. It also explains why the E_{kin} error in the sm4thpoly method is actually as large as the pom2nd method (Fig. 7b).

The general error behaviors for the sixth-order schemes, see Fig. 8, are similar to those described above for the fourth-order methods (i.e., Fig. 7). Also, consistent with the findings in the seamount tests that sixth-order methods do not necessarily give reduced errors, a comparison of Fig. 8 with Fig. 7 shows that, in this realistic northwest Atlantic experiment, the sixth-order methods actually yield larger errors. In view of this result (and the increased complexity of the sixth-order methods), and the fact that the fourth-order methods do give an order of magnitude smaller averaged errors than the standard second-order POM (Fig. 7b), the fourth-order methods are particularly attractive.

The advantage of using the fourth-order methods may be demonstrated by giving the depth-integrated transport stream function (in Sv; 1 Sv = 10^6 m^3 s^{-1}) over the model domain for the pom2nd method, the fourth-order POM methods, and the sm4thCubicH method, see Fig. 9. Plots for the sm4thpoly and the pom6th methods are also included, although these methods yielded poorer results than the other fourth-order methods. Large IPG errors exist for the second-order POM method over steep slopes and trenches north and east of the Bahamas and the Windward Islands, and also at isolated locations in the Caribbean Sea (Fig. 9a). Cyclonic (red) and anticyclonic (blue) transports with maxima of about 4 Sv are seen. With the fourth-order methods, these errors are mostly eliminated, and only an isolated error of O(1–2 Sv) magnitude remains near Jamaica (i.e., south of Cuba); here, the grid size is very coarse, of O(40 km). Over the other regions, the IPG errors are smaller, less than 1 Sv. The POM fourth-order methods (both McCalpin and compact differencing) give very similar error distributions. In comparing the sm4thCubicH method (Fig. 9d) with the fourth-order POM methods (Fig. 9b or c), we see that the former has slightly larger error (lighter green, just under 1 Sv) over wider regions of the domain than the latter (darker green, about 0.3 Sv). This was mentioned previously in conjunction with the smaller E_{kin} error in the case of the POM fourth-order methods when compared with the SM03 Cubic-H method (Fig. 7b). The basin-averaged absolute stream functions are least for pom4thMcC and pom4thCmp, both at 0.11 Sv; the

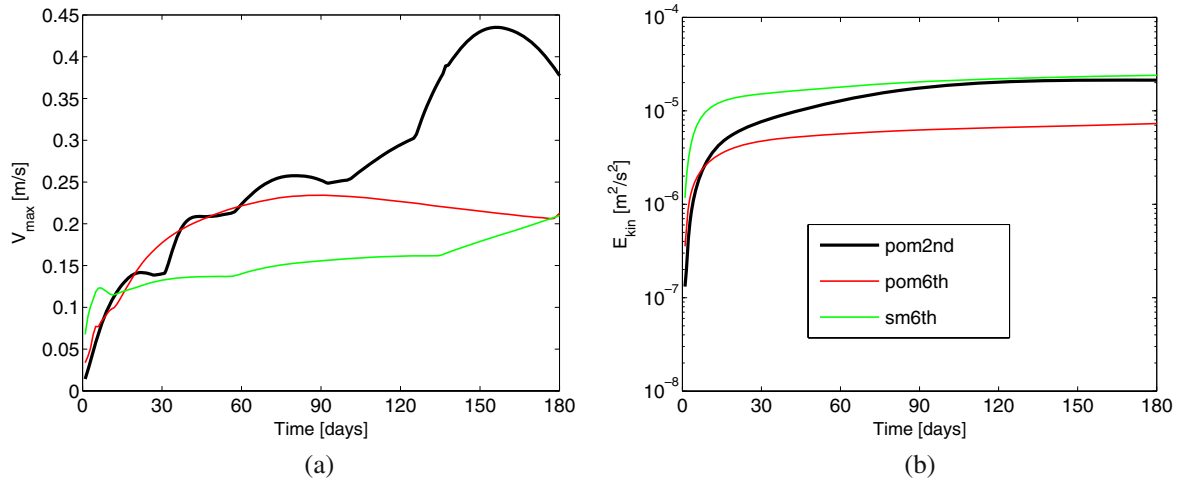

Fig. 8 Time series of V_{max} and E_{kin} for Northwest Atlantic experiment, for the pom2nd method and the two sixth-order methods (**a**, **b**)

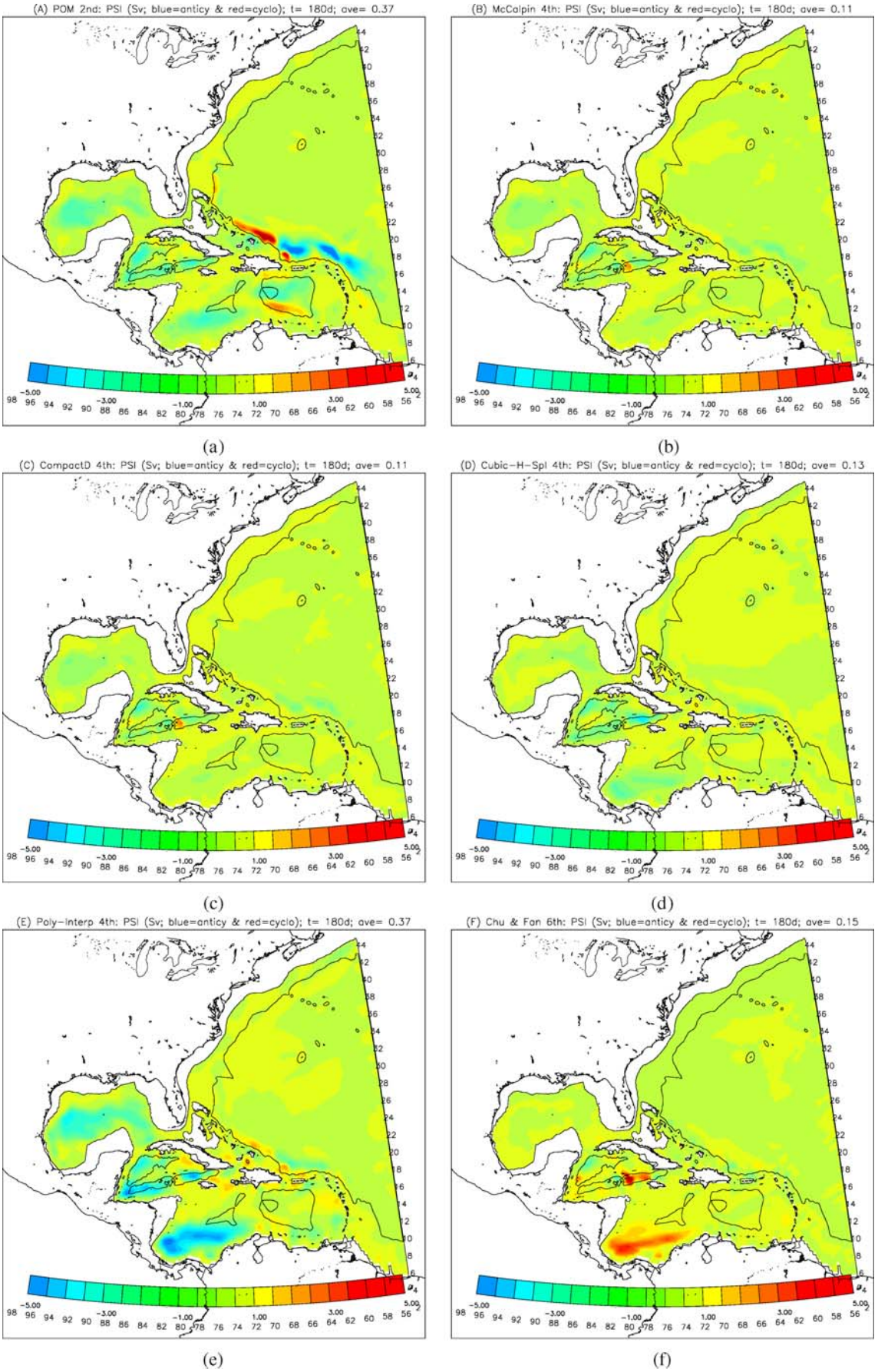
(A) POM 2nd: PSI (Sv; blue=anticy & red=cyclo); t= 180d; ave= 0.37
(B) McCalpin 4th: PSI (Sv; blue=anticy & red=cyclo); t= 180d; ave= 0.11
(a)
(b)
(C) CompactD 4th: PSI (Sv; blue=anticy & red=cyclo); t= 180d; ave= 0.11
(D) Cubic-H-Spl 4th: PSI (Sv; blue=anticy & red=cyclo); t= 180d; ave= 0.13
(c)
(d)
(E) Poly-Interp 4th: PSI (Sv; blue=anticy & red=cyclo); t= 180d; ave= 0.37
(F) Chu & Fan 6th: PSI (Sv; blue=anticy & red=cyclo); t= 180d; ave= 0.15
(e)
(f)

◀ **Fig. 9** Stream functions (+ for cyclonic circulation) after 180 days for **a** the pom2nd method, **b** the pom4thMcC method, **c** the pom4thCmp method, **d** the sm4thCubicH method, **e** the sm4thpoly method, and **f** the pom6th method. For clarity, small values for water depths less than 200 m are omitted

error is 0.13 Sv for sm4thCubicH, and is 0.37 Sv for pom2nd. The absolute stream function error is 0.37 Sv for sm4thpoly, and is 0.15 Sv for pom6th. As commented above, the sm4thpoly method performs poorly, while the sixth-order methods (same with sm6th, not shown) yield worse results than the more efficient fourth-order methods.

5 Conclusion

In the present paper, POM approach methods for estimating the IPGs in σ-coordinate ocean models are compared to the corresponding methods based on the integral approach suggested in Shchepetkin and McWilliams (2003). In order to separate out the effects of higher order from the effects of the basic integral approach, methods to the same order of accuracy are compared and a sixth-order method based on the SM03 approach is derived to facilitate the comparison. We find that the errors may be substantially reduced by using one of the fourth-order POM methods, the McCalpin (1994) method, or the fourth-order compact differencing method, rather than the second-order POM method. The fourth-order SM03 methods are generally less robust than the fourth-order POM methods. However, the fourth-order POM methods are only marginally more accurate than the fourth-order SM03 Cubic-H method in the realistic case. It may accordingly be difficult to identify an overall "best" method, see also the results and discussions in Kliem and Pietrzak (1999), Berntsen and Thiem (2007), and SM03. It will be the sum of numerical evidence provided in this and other similar work that points towards robust and good methods. With several good candidates for the estimation of the IPGs to choose from, other criteria like computational cost may also be considered.

A change from the standard second-order POM method to a higher-order method increases the computational complexity. When using the compact differencing fourth-order method, the computational stencil becomes as wide as the computational domain, and the solution of tridiagonal systems of equations is involved. The Cubic-H method from SM03 involves more algebraic operations than the McCalpin method and the Cubic-H method requires tests on the signs of the local derivatives, see Section 5 in SM03. Such tests may reduce the computational efficiency, especially on vector processors. The computational times for 2-day integration of the seamount problem (Table 1) indicate that the cost for using higher-order schemes such as the pom4thMcC and the sm4thCubicH is only 6% to 8% more than the pom2nd. We find that, for longer integrations of 100 days or more, and especially when using the full model (instead of the simplified version used here), the pressure gradient estimation is but a small portion of the model calculation, and the additional costs become insignificant. The computational stencil of the fourth-order McCalpin (1994) method involves two more points than the second-order POM method. It is, however, still much simpler than other fourth-order methods. The IPG errors are substantially reduced when using the McCalpin method rather than the second-order POM method. The results from the present numerical exercises suggest that this method is robust and performs favorably compared to the other fourth-order methods. The fourth-order McCalpin (1994) method also performed well in the numerical exercises for the Nordic Seas on IPG errors reported in Berntsen and Thiem (2007).

It is not clear that the errors are further reduced when extending from fourth to sixth order, especially in long time integrations. The sixth-order Chu and Fan (1997) method seems to be more robust than the new sixth-order method based on the SM03 approach.

Finally, in real applications, there are techniques such as topography smoothing and the subtraction of the area-averaged mean density profile that can reduce the IPG errors, see the discussion in Section 1. The IPG errors are also reduced as we use higher spatial resolution. In a recent study of tidal flow over a sill, for example, the maximum IPG error was 1×10^{-4} ms^{-1}, whereas the maximum tidal velocity over the sill was 0.65 ms^{-1}, see Berntsen et al. (2008). That study was done with a horizontal grid size of 12.5 m. In such high-resolution exercises, there are other sources of errors such as details in the topography and parameterization of subgrid scale processes that are more critical.

Acknowledgements The authors thank two reviewers and the editor for constructive remarks. The first author has received support from The Research Council of Norway through the CORDINO project grant 146526/420. The second author was partially supported by Minerals Management Service contract numbers M08PC20007.

Appendix: The sixth-order method using Green's theorem approach

To extend the methods based on Green's theorem approach to sixth order, statement (5.5) in SM03 is extended to include up to fifth-order terms

$$f(\xi) = f^{(0)} + f^{(1)}\xi + f^{(2)}\frac{\xi^2}{2} + f^{(3)}\frac{\xi^3}{6} + f^{(4)}\frac{\xi^4}{24} + f^{(5)}\frac{\xi^5}{120}. \tag{16}$$

When it is required that the polynomial fit to the values in the grid points, the six coefficients in the equation become

$$\begin{aligned}
f^{(0)} &= \frac{75}{128}(f_{1/2} + f_{-1/2}) - \frac{25}{256}(f_{3/2} + f_{-3/2}) + \frac{3}{256}(f_{5/2} + f_{-5/2}) \\
f^{(1)} &= \frac{75}{64}(f_{1/2} - f_{-1/2}) - \frac{25}{384}(f_{3/2} - f_{-3/2}) + \frac{3}{640}(f_{5/2} - f_{-5/2}) \\
f^{(2)} &= -\frac{17}{24}(f_{1/2} + f_{-1/2}) + \frac{13}{16}(f_{3/2} + f_{-3/2}) - \frac{5}{48}(f_{5/2} + f_{-5/2}) \\
f^{(3)} &= -\frac{17}{4}(f_{1/2} - f_{-1/2}) + \frac{13}{8}(f_{3/2} - f_{-3/2}) - \frac{1}{8}(f_{5/2} - f_{-5/2}) \\
f^{(4)} &= (f_{1/2} + f_{-1/2}) - \frac{3}{2}(f_{3/2} + f_{-3/2}) + \frac{1}{2}(f_{5/2} + f_{-5/2}) \\
f^{(5)} &= 10(f_{1/2} - f_{-1/2}) - 5(f_{3/2} - f_{-3/2}) + (f_{5/2} - f_{-5/2}),
\end{aligned} \tag{17}$$

which corresponds to equation (5.6) in SM03.

To obtain a sixth-order method, three more terms must be added to the terms on the right-hand side of equation (5.10) in SM03 as follows:

$$\begin{aligned}
\int_{-1/2}^{1/2} \rho\frac{\partial z}{\partial \xi}d\xi = {} & \rho^{(0)}z^{(1)} + \frac{1}{24}\rho^{(0)}z^{(3)} + \frac{1}{24}\rho^{(2)}z^{(1)} \\
& + \frac{1}{12}\rho^{(1)}z^{(2)} + \frac{1}{320}\rho^{(2)}z^{(3)} + \frac{1}{480}\rho^{(3)}z^{(2)} \\
& + \frac{1}{1920}\rho^{(0)}z^{(5)} + \frac{1}{480}\rho^{(1)}z^{(4)} \\
& + \frac{1}{1920}\rho^{(4)}z^{(1)}.
\end{aligned} \tag{18}$$

Estimating the integral along the horizontal lines, see statement (5.4) in SM03, to second order, we get the following approximation:

$$\begin{aligned}
FC_{i+1/2,k} &= \int_{\xi_{i,k}}^{\xi_{i+1,k}} \rho\frac{\partial z}{\partial \xi}d\xi \\
&= \frac{1}{2}(\rho_{i+1,k} + \rho_{i,k})(z_{i+1,k} - z_{i,k}),
\end{aligned} \tag{19}$$

which is the same as the leading term given in Section 5.1, Remark 7 in SM03. Statement (5.6) from SM03 may be used to correct the second-order approximation above to fourth-order accuracy, and the following terms must be added to the approximation:

$$\begin{aligned}
& \frac{5}{128}(\rho_{i+1,k} + \rho_{i,k})(z_{i+1,k} - z_{i,k}) \\
& + \frac{1}{1152}(\rho_{i+1,k} + \rho_{i,k})(z_{i+2,k} - z_{i-1,k}) \\
& - \frac{5}{128}(\rho_{i+2,k} + \rho_{i-1,k})(z_{i+1,k} - z_{i,k}) \\
& - \frac{1}{1152}(\rho_{i+2,k} + \rho_{i-1,k})(z_{i+2,k} - z_{i-1,k}) \\
& + \frac{3}{64}(\rho_{i+1,k} - \rho_{i,k})(z_{i+2,k} - z_{i+1,k} - z_{i,k} + z_{i-1,k}) \\
& - \frac{1}{576}(\rho_{i+2,k} - \rho_{i-1,k})(z_{i+2,k} - z_{i+1,k} - z_{i,k} + z_{i-1,k}).
\end{aligned} \tag{20}$$

Using the expressions for $f^{(0)}$ to $f^{(5)}$ given above, the approximation may be corrected to sixth-order accuracy by adding the following 18 terms:

$$
\begin{aligned}
&\frac{2741}{122880}(\rho_{i+1,k}+\rho_{i,k})(z_{i+1,k}-z_{i,k})\\
&\quad-\frac{5701}{2211840}(\rho_{i+1,k}+\rho_{i,k})(z_{i+2,k}-z_{i-1,k})\\
&\quad+\frac{173}{1228800}(\rho_{i+1,k}+\rho_{i,k})(z_{i+3,k}-z_{i-2,k})\\
&\quad-\frac{2509}{81920}(\rho_{i+2,k}+\rho_{i-1,k})(z_{i+1,k}-z_{i,k})\\
&\quad+\frac{4189}{1474560}(\rho_{i+2,k}+\rho_{i-1,k})(z_{i+2,k}-z_{i-1,k})\\
&\quad-\frac{133}{819200}(\rho_{i+2,k}+\rho_{i-1,k})(z_{i+3,k}-z_{i-2,k})\\
&\quad+\frac{409}{49152}(\rho_{i+3,k}+\rho_{i-2,k})(z_{i+1,k}-z_{i,k})\\
&\quad-\frac{233}{884736}(\rho_{i+3,k}+\rho_{i-2,k})(z_{i+2,k}-z_{i-1,k})\\
&\quad+\frac{53}{2457600}(\rho_{i+3,k}+\rho_{i-2,k})(z_{i+3,k}-z_{i-2,k})\\
&\quad-\frac{313}{23040}(\rho_{i+1,k}-\rho_{i,k})(z_{i+1,k}+z_{i,k})\\
&\quad+\frac{83}{3840}(\rho_{i+1,k}-\rho_{i,k})(z_{i+2,k}+z_{i-1,k})\\
&\quad-\frac{37}{4608}(\rho_{i+1,k}-\rho_{i,k})(z_{i+3,k}+z_{i-2,k})\\
&\quad-\frac{59}{138240}(\rho_{i+2,k}-\rho_{i-1,k})(z_{i+1,k}+z_{i,k})\\
&\quad+\frac{13}{46080}(\rho_{i+2,k}-\rho_{i-1,k})(z_{i+2,k}+z_{i-1,k})\\
&\quad+\frac{1}{6912}(\rho_{i+2,k}-\rho_{i-1,k})(z_{i+2,k}+z_{i-1,k})\\
&\quad-\frac{19}{230400}(\rho_{i+3,k}-\rho_{i-2,k})(z_{i+1,k}+z_{i,k})\\
&\quad+\frac{7}{76800}(\rho_{i+3,k}-\rho_{i-2,k})(z_{i+2,k}+z_{i-1,k})\\
&\quad-\frac{1}{115200}(\rho_{i+3,k}-\rho_{i-2,k})(z_{i+3,k}+z_{i-2,k}). \qquad (21)
\end{aligned}
$$

Similarly, one may approximate the vertical integrals, $FX_{i,k+1/2}$ in SM03, to sixth order. However, given an adequate vertical resolution, the use of the second-order trapezoidal rule for the vertical integrals is sufficient. The main focus in the present paper is accordingly on higher-order methods for the horizontal approximations.

References

Barnier B, Marchesiello P, de Miranda A, Molines J-M, Coulibaly M (1998) A sigma-coordinate primitive equation model for studying the circulation in the South Atlantic. Part I: model configuration with error estimates. Deep-Sea Res I 45:543–572

Beckmann A, Haidvogel D (1993) Numerical simulation of flow around a tall isolated seamount. Part I: problem formulation and model accuracy. J Phys Oceanogr 23:1736–1753

Berntsen J (2002) Internal pressure errors in sigma-coordinate ocean models. J Atmos Ocean Technol 19(9):1403–1414

Berntsen J, Furnes G (2005) Internal pressure errors in sigma-coordinate ocean models- sensitivity of the growth of the flow to the time stepping method and possible non-hydrostatic effects. Cont Shelf Res 25:829–848

Berntsen J, Thiem Ø (2007) Estimating the internal pressure gradient errors in a σ-coordinate ocean model for the Nordic Seas. Ocean Dyn 57:417–429

Berntsen J, Xing J, Davies A (2008) Numerical studies of internal waves at a sill: sensitivity to horizontal size and subgrid scale closure. Cont Shelf Res 28:1376–1393

Blumberg A, Mellor G (1987) A description of a three-dimensional coastal ocean circulation model. In: Heaps N (ed) Three-dimensional coastal ocean models. Coastal and Estuarine Series, vol 4. American Geophysical Union, Washington, DC, pp 1–16

Chu P, Fan C (1997) Sixth-order difference scheme for sigma coordinate ocean models. J Phys Oceanogr 27:2064–2071

Chu P, Fan C (2003) Hydrostatic correction for sigma coordinate ocean models. J Geophys Res 108:3206–3218

Ciappa A (2006) An operational comparative test of z-levels PGF schemes to reduce pressure gradient errors of the ocean model POM. Ocean Model 12:80–100

Di Lorenzo E, Young W, Smith S (2006) Numerical and analytical estimates of M_2 tidal conversion at steep oceanic ridges. J Phys Oceanogr 36:1072–1084

Ezer T, Arango H, Shchepetkin A (2002) Developments in terrain-following ocean models: intercomparisons of numerical aspects. Ocean Model 4:249–267

Fortunato A, Baptista A (1996) Evaluation of horizontal gradients in sigma-coordinate shallow water models. Atmos-ocean 34:489–514

Gary J (1973) Estimation of truncation errors in transformed coordinate, primitive equation atmospheric models. J Atmos Sci 30:223–233

Haney R (1991) On the pressure gradient force over steep topography in sigma coordinate ocean models. J Phys Oceanogr 21:610–619

Kantha L, Clayson C (2000) Numerical models of oceans and oceanic processes. In: International geophysics series, vol 66. Academic, London

Kliem N, Pietrzak J (1999) On the pressure gradient error in sigma coordinate ocean models: a comparison with a laboratory experiment. J Geophys Res 104:29781–29799

McCalpin J (1994) A comparison of second-order and fourth-order pressure gradient algorithms in a σ-coordinate ocean model. Int J Numer Methods Fluids 18:361–383

Mellor G (2003) Users guide for a three-dimensional, primitive equation, numerical ocean model. Technical report, Princeton University

Mellor G, Ezer T, Oey L-Y (1994) The pressure gradient conundrum of sigma coordinate ocean models. J Atmos Ocean Technol 11:1126–1134

Mellor G, Oey L-Y, Ezer T (1998) Sigma coordinate pressure gradient errors and the seamount problem. J Atmos Ocean Technol 15:1122–1131

Oey L-Y, Lee H-C, Schmitz W Jr (2003) Effects of winds and Caribbean eddies on the frequency of loop current eddy shedding: a numerical study. J Geophys Res 108(C10):3324. doi:10.1029/2002JC001698

Orzag S, Israeli M (1974) Numerical simulation of viscous incompressible flows. Annu Rev Fluid Mech 6:282–318

Robertson R, Padman L, Levine M (2001) A correction to the baroclinic pressure gradient term in the Princeton ocean model. J Atmos Ocean Technol 18:1068–1075

Shchepetkin A, McWilliams J (2003) A method for computing horizontal pressure-gradient force in an oceanic model with a non-aligned vertical coordinate. J Geophys Res 108(C3, 3090). doi:10.1029/2001C001047

Sikirić M, Janeković I, Kuzmić M (2009) A new approach to bathymetry smoothing in sigma-coordinate ocean models. Ocean Model 29:128–136

Slørdal L (1997) The pressure gradient force in sigma-coordinate ocean models. Int J Numer Methods Fluids 24:987–1017

Song Y (1998) A general pressure gradient formulation for ocean models. Part I: scheme design and diagnostic analysis. Mon Weather Rev 126:3213–3230

Song Y, Wright D (1998) A general pressure gradient formulation for ocean models. Part II: energy, momentum and bottom torque consistency. Mon Weather Rev 126:3231–3247

Stelling G, Van Kester J (1994) On the approximation of horizontal gradients in sigma coordinates for bathymetry with steep bottom slopes. Int J Numer Methods Fluids 18:915–935